RSC Advances

PAPER

View Article Online
View Journal | View Issue

Check for updates

Cite this: *RSC Adv.*, 2018, **8**, 25846

Ni or Ru supported on MgO/γ-Al_2O_3 pellets for the catalytic conversion of ethanol into butanol

J. Apuzzo, S. Cimino and L. Lisi *

Received 21st May 2018
Accepted 10th July 2018

DOI: 10.1039/c8ra04310h

rsc.li/rsc-advances

Ni- and Ru-based catalytic pellets supported on commercial γ-Al_2O_3 pellets modified with magnesium oxide have been prepared for application in the catalytic conversion of ethanol into butanol. MgO/γ-Al_2O_3 pellets with or without added metals have been characterized by XRD, SEM/EDX, TGA, N_2 physisorption, H_2 TPR, and CO_2 TPD in order to investigate the effect of MgO coverage and metal distribution on the surface and red-ox properties of the materials and, in turn, their effects on the catalytic performance. The conversion of ethanol into butanol has been investigated in a continuous flow reactor at 350–400 °C under diluted conditions (3% ethanol) in order to rank the different catalytic pellets and identify the best formulations and preparation procedures *via* a comparison with powder catalysts previously proposed in the literature with similar compositions. Results show enhanced catalytic performance for MgO-covered alumina pellets with respect to a pure MgO powder catalyst in spite of the lower MgO load. A significant further positive effect is found when Ni or Ru enters a solid solution with MgO.

Open Access Article. Published on 18 July 2018. Downloaded on 7/14/2025 8:34:56 AM.
This article is licensed under a Creative Commons Attribution-NonCommercial 3.0 Unported Licence.

1. Introduction

The addition of bio-ethanol to gasoline is limited by issues such as water solubility and corrosivity which would require its substitution for a higher fuel-soluble alcohol such as butanol.[1] Bio-butanol can be produced by biomass fermentation with *Clostridium* microorganisms (Acetone Butanol Ethanol or ABE fermentation).[2] The fraction of ethanol produced according to this method could be upgraded through suitable processes.

The Guerbet reaction is an alcohol dimerization to form a higher alcohol.[3] The alcohol can react with itself or with another alcohol with the loss of one water molecule. Dimerization of ethanol leads to butanol, however, the reaction selectivity represents a critical issue due to the formation of significant amounts of by-products such as acetaldehyde and ethylene.[3] The process is generally activated by a large variety of catalysts ranging from supported metals (Ru, Rh, Pd, Pt, Au, Ni, Ag),[4,5] hydroxyapatite (HAP)[6–8] and to basic oxides such as MgO.[9–12]

Nevertheless, a preliminary screening of powder catalysts belonging to these categories carried out by us under diluted ethanol conditions[13] did not confirm results previously reported in the literature concerning Al_2O_3- and HAP-based materials. In fact, these two materials only promoted the formation of by-products,[13] whereas metal-promoted MgO was identified as the catalyst providing the best butanol yields. More in detail, the addition of Ni or Ru to MgO increased both the surface area and number and strength of basic sites related to an enhanced butanol productivity. The key role of basic sites was well evidenced by Birky *et al.*[14] who performed both CO_2 adsorption and ethanol adsorption tests on the MgO surface by DRIFT studies under Guerbet reaction steady-state conditions. They found a high ethanol surface coverage, largely exceeding that of CO_2, which was activated as ethoxy at 400 °C. On the basis of their results, they supposed that strong basic sites facilitate the formation of butanol, presumably through a coupling reaction giving the aldol condensation while inhibiting the C–C coupling reactions to C6 and heavier compounds that deactivates the catalyst at high temperature.

Likewise, it was found by other authors, for MgO and Mg–Al mixed oxides, that a high concentration and strength of the basic sites are associated to good selectivity to 1-butanol whereas acid sites promote dehydration of ethanol.[15–17] Chieregato *et al.* reported that the Guerbet coupling over MgO starts with dehydrogenation of the alcohol to form the carbonyl intermediate and suggested that the addition of a metal with hydrogenation/dehydrogenation properties can promote this step.[16]

The preliminary work described in a previous paper,[13] carried out on powder catalysts in a lab-scale rig, has been followed in the present work by the attempt to reproduce the MgO-based catalysts in a structured form (pellets) to be used in a larger scale rig.

On the basis of our previous results[13] and on data about Mg–Al mixed oxides,[15,17] the choice fell on γ-Al_2O_3 pellets as the scaffold of metal-promoted MgO catalysts. The main

Istituto di Ricerche sulla Combustione, CNR, P.le Tecchio 80, 80125 Napoli, Italy. E-mail: luciana.lisi@cnr.it

This journal is © The Royal Society of Chemistry 2018

Open Access Article. Published on 18 July 2018. Downloaded on 7/14/2025 8:34:56 AM.
This article is licensed under a Creative Commons Attribution-NonCommercial 3.0 Unported Licence.

reasons that supported this choice were: (i) preliminary attempts to disperse metals on MgO pellets gave poorly reproducible results as concerns surface area strongly depending on calcination temperature (ii) γ-Al_2O_3 provides a large surface area to disperse MgO significantly enhancing its exposure to ethanol (iii) a synergic effect between Al and Mg can be supposed improving performance.[15,17]

Dispersion of nickel on magnesia has been widely investigated due to the possible interactions occurring between Ni^{2+} and MgO.[18–22] Many authors claimed the migration of Ni^{2+}into MgO structure which is enhanced by higher calcination temperature.[18,19] Also Ru deposition on MgO or mixed oxide Mg–Al was reported with magnesium promoting ruthenium dispersion.[23–28]

Most of these studies are focused on powder catalysts. Nevertheless, possible concerns related to the distribution of the metal along the radius of a support in a spherical or cylindrical form, as pellets, has been scarcely tackled. Some authors reported the preparation of Ni-based catalysts with an egg-shell metal distribution purposely obtained for catalysis for very fast reaction with mass transfer limitations.[29–31] In particular, Qiu *et al.* dispersed a Ni layer onto MgO/Al_2O_3 spheres pre-calcined at different temperatures.[29]

In this work we set out to investigate the preparation and characterization of Ni and Ru on MgO-coated γ-Al_2O_3 pellets as structured catalysts for the ethanol coupling reaction. In particular, the effect of some specific preparation steps was assessed with regards to the dispersion of the metals in the pellets, interaction with the alumina support and formation/stabilization of best performing active phases.

2. Experimental

2.1 Preparation of catalytic pellets

MgO/γ-Al_2O_3 pellets were prepared by incipient wetness impregnation of γ-Al_2O_3 pellets NORPRO supplied by Saint-Gobain (1/8 inch) using a water solution of $Mg(NO_3)_2\cdot 6H_2O$ (Sigma-Aldrich) with such a concentration designed to obtain a nominal loading of either 12 wt% MgO. After drying at 120 °C, pellets were calcined in air for 2 h at 600 °C, and part of them was further calcined for 2 h at 900 °C. Pellets with a nominal loading of 20% MgO were prepared by performing a second impregnation–calcination cycle.

Nickel was dispersed by incipient wetness impregnation starting from a water solution of $Ni(NO_3)\cdot 6H_2O$ (Fluka, 98.5% purity), whereas ruthenium was dispersed starting from a 1.4% wt ruthenium(III) nitrosyl nitrate solution (Aldrich). The nominal loadings of Ni and Ru in the pellets were fixed at 1% and 0.5% wt, respectively.

Hereafter, the catalysts will be labelled as Me/*x*Mg/Al, where Me represents the specific metal (Ni or Ru) and *x* the MgO weight percentage. Moreover, Ni (1%) was also supported on pure MgO pellets (Harshaw, 1/8 inch) by incipient wetness impregnation using a water solution of the metal nitrate. Eventually, a reference MgO powder was also prepared by precipitation using $Mg(NO_3)\cdot 6H_2O$ and NH_3 as previously described.[13]

2.2 Characterization of pellets

A TG/FTIR analysis under air flow simulating the calcination step up to 600 °C was carried out using a Setaram TGA Labsys Evo coupled to a Perkin-Elmer Spectrum GX spectrometer.

XRD analysis was performed on powdered samples with a Bruker D2 Phaser diffractometer operated at diffraction angles ranging between 10 and 80° 2θ with a scan velocity equal to 0.02° 2θ s^{-1}.

Specific surface area and pore size distribution of the catalysts were evaluated by N_2 adsorption at 77 K according to the BET and BJH models respectively, in a Quantachrome Autosorb 1-C after degassing samples for 2 h at 150 °C.

The actual metal loading of the catalysts was verified by ICP-MS using an Agilent 7500 instrument after MW assisted acid digestion.

Scanning electron microscopy (SEM) of cross-sectioned pellets was carried out with a FEI Inspect instrument equipped with an energy dispersive X-ray (EDX) probe.

Temperature programmed reduction (TPR) experiments were carried out with a Micromeritics AutoChem 2020 equipped with a TC detector on catalysts and supports pre-treated in air at 600 °C. The sample (150 mg) was heated at 10 °C min^{-1} between room temperature and 900 °C under a flow of 2% H_2/N_2 mix (50 cm^3 min^{-1}). CO_2 temperature programmed desorption (TPD) experiments were performed in the same apparatus, by heating samples up to 600 °C at 10 °C min^{-1} under He flow (50 cm^3 min^{-1}), after adsorption of 15% CO_2/N_2 mix at room temperature.

2.3 Catalytic test

Catalytic tests were carried out at 350 and 400 °C by feeding a 3% vol. ethanol/N_2 mixture (3 L h^{-1}) to a lab-scale fixed bed reactor containing 1 g of catalytic pellets and operated at nearly atmospheric pressure, under pseudo-isothermal conditions. A main N_2 flow was bubbled through liquid ethanol in a saturator and the exit ethanol concentration was determined by the Antoine equation. An additional pure N_2 flow dilutes this main stream with such a ratio to obtain 3% ethanol in the total feed stream, as previously described.[13] Reactants and products were analysed by an online GC (Hewlett Packard) equipped with FI detector and a ZB-WAXplus column. All species were separated except for ethylene from diethyl ether. Percentage butanol yield was expressed as butanol produced/ethanol reacted ×100 (vol/vol). GC peak areas were evaluated within 5% experimental error.

3. Results and discussion

3.1 Characterization of supports

TG-FTIR analysis during the calcination treatment of dried *x*Mg/Al pellets (not shown) revealed that the decomposition of the impregnated nitrate precursor occurred in the temperature range 300–400 °C. In fact, in correspondence of weight loss occurring in this temperature range, the typical IR bands of NO_2 were observed at 1580–1650 cm^{-1}. That is in agreement with results of Qiu *et al.*[29] who found that IR signals of nitrate groups

Open Access Article. Published on 18 July 2018. Downloaded on 7/14/2025 8:34:56 AM.
This article is licensed under a Creative Commons Attribution-NonCommercial 3.0 Unported Licence.

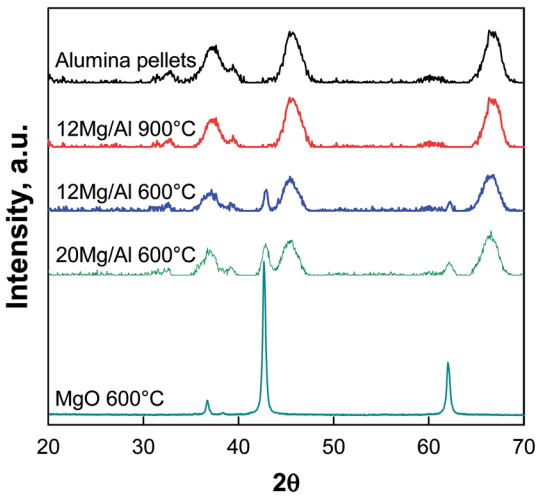

Fig. 1 XRD patterns of *x*Mg/Al pellets calcined at 600 and 900 °C compared to MgO powder and γ-Al_2O_3 pellets calcined at 600 °C.

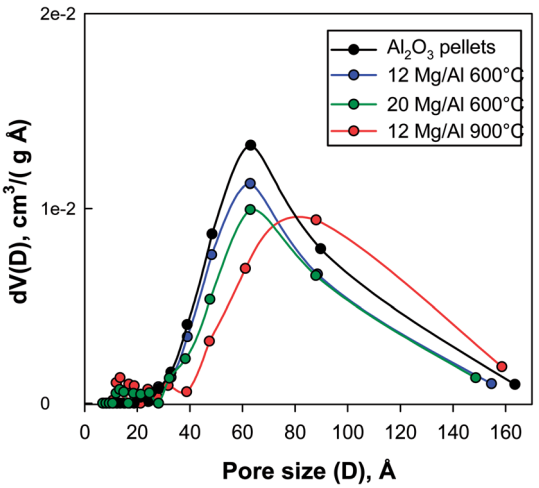

Fig. 2 Effect of MgO addition (12 or 20% wt) and calcination temperature (600 or 900 °C) on the pore size distribution of γ-Al_2O_3 pellets.

from $Mg(NO_3)_2$ precursor used for impregnation of γ-Al_2O_3 spheres were still present if the composite support was calcined at 350 °C whereas they disappeared after heating at 450 °C. In our experiment at 550–600 °C a stable weight was achieved thus ensuring that nitrates are totally decomposed at the calcination temperature.

In Fig. 1 XRD patterns of 12Mg/Al pellets calcined at 600 or 900 °C are compared with those of pure γ-Al_2O_3 pellets and pure MgO powder treated at 600 °C.

The γ-alumina structure of the commercial pellets was substantially preserved in both patterns of MgO-containing pellets. In addition to the signals of γ-Al_2O_3, the main reflections of periclase MgO phase at 42.9° and 62.3° (JCPDS 45-946) were detected for 12 Mg/Al and particularly for 20Mg/Al samples calcined at 600 °C. On the other hand, for 12Mg/Al the pellets calcined at 900 °C those signals disappeared suggesting the formation of a surface spinel-like $MgAl_2O_4$ structure[32] due to the migration of Mg^{2+} into alumina lattice taking place at 900 °C.

The values of the BET surface area (Table 1) indicate that MgO addition decreased the original surface area of alumina, mostly as expected by the weight increase of the pellets. Calcination at 900 °C induced a further but limited reduction of the BET area. Moreover, as shown in Fig. 2, the original pore size distribution of γ-Al_2O_3, characterized by a clear maximum centred around 60 Å, was preserved when the calcination temperature was limited to 600 °C regardless of the MgO loading on the pellets. On the other hand, the calcination at 900 °C induced an enlargement of the mean pore diameter up to *ca.* 90 Å, in good agreement to the effect of the formation of $MgAl_2O_4$ spinel reported by Qiu *et al.*[29]

Temperature Programmed Desorption (TPD) of CO_2 was used as a fingerprint to evaluate the typical distribution of basic sites of the materials: in Fig. 3, CO_2 TPD profiles of *x*Mg/Al pellets calcined at 600 and 900 °C are compared with those relevant to pure MgO powder and γ-Al_2O_3 pellets calcined at 600 °C. Notably, markedly different profiles were recorded for the two 12 Mg/Al samples depending on the temperature of calcination. The one prepared at 600 °C showed an asymmetric peak centred at 115–120 °C with a long tail extending up to 600 °C. On the contrary, 12Mg/Al sample calcined at 900 °C displayed two peaks with maxima at 130 and 515 °C, respectively. Such a double peak profile closely resembles the one recorded for commercial γ-Al_2O_3 pellets and, as a consequence, confirms that calcination at high temperature promoted the formation of a spinel-like structure with the inclusion of Mg into the Al_2O_3 lattice, in agreement with XRD and porosimetric analyses. On the other hand, the CO_2 TPD profile for pure MgO powder showed a main peak at *ca.* 210 °C extending up to 450 °C with a shoulder at *ca.* 130 °C. Inspection of relevant profiles for 12 Mg/Al and 20Mg/Al pellets calcined at 600 °C indicates that

Table 1 BET surface area and basic sites evaluated through CO_2 TPD of Mg/Al pellets calcined at different temperatures

Sample	Shape size	Calcination temperature (°C)	BET surface area ($m^2\ g^{-1}$)	Pore volume ($cm^3\ g^{-1}$)	Basic sites (CO_2 TPD) (mmol g^{-1})
γ-Al_2O_3	Pellets 1/8 inch	600	169	0.78	0.16
MgO	Powder	600	26	0.15	0.064
12Mg/Al	Pellets 1/8 inch	600	141	0.68	0.34
12Mg/Al	Pellets 1/8 inch	900	127	0.70	0.18
20Mg/Al	Pellets 1/8 inch	600	115	0.62	0.40

This journal is © The Royal Society of Chemistry 2018

Open Access Article. Published on 18 July 2018. Downloaded on 7/14/2025 8:34:56 AM.
This article is licensed under a Creative Commons Attribution-NonCommercial 3.0 Unported Licence.

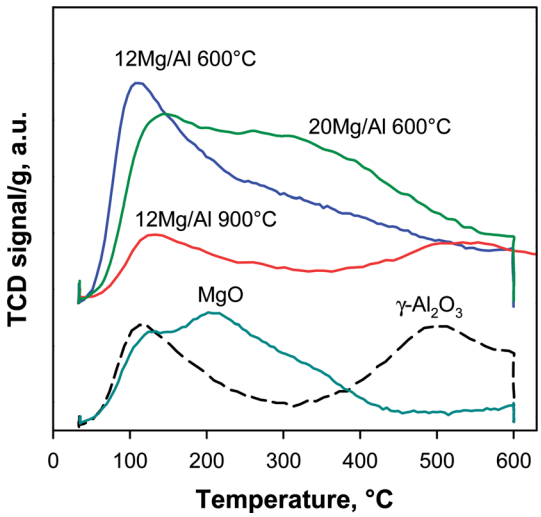

Fig. 3 CO_2 TPD profiles of *x*Mg/Al pellets calcined at 600 and 900 °C compared with γ-Al_2O_3 pellets and pure MgO powder treated at 600 °C.

they included all typical contributions from basic sites of both MgO and Al_2O_3, confirming the formation of the former phase on the surface of the latter. As expected, the number of basic sites increased with MgO content in the pellets, with a stronger contribution to CO_2 desorption in the temperature range from 200 to 450 °C. Quantitative analysis of TPD profiles (Table 1) confirmed the large increase of basic sites upon MgO addition to alumina pellets calcined at 600 °C, whereas calcination at 900 °C promoted the formation of a material with features very similar to that of γ-Al_2O_3. Furthermore, a direct comparison of the amount of CO_2 desorbed from MgO-coated alumina pellets and from pure MgO highlights that the total number of exposed basic sites per gram of sample was increased by as much as 5–6 times through superficial dispersion of MgO. However, the amount of basic sites estimated in this work is lower than that reported by León *et al.* for Mg/Al mixed oxides having a similar surface area but a higher Mg/Al ratio (*ca.* 3×).[17] On the contrary, both 12Mg/Al and 20 Mg/Al have a higher density of basic sites with respect to that evaluated by Birky *et al.*[14] for pure MgO (2.4 and 3.5 × 10^{-6} mol m^{-2} respectively *vs.* 1.0 × 10^{-6} mol m^{-2}).

3.2 Characterization of catalytic pellets

As mentioned in the Introduction, dispersion of active metals represented a crucial step in the preparation of catalytic pellets due to the risk of poor penetration of the metal deep in the body of the pellets, which, in principle, could reduce the overall catalytic performance of the system. In fact, this phenomenon was well evident when using pure MgO pellets as a support. A significant segregation of Ni on the outer surface of the pellet was observed producing an egg-shell type distribution of the metal across the section of pure MgO pellets (Fig. 4a and a′).

That is mostly assignable to the precipitation of $Ni(OH)_2$ from the nitrate precursor solution at the first contact with the very basic MgO surface that precluded any significant penetration of nickel inside the pellet structure. Attempts to promote metal diffusion in the porous structure, such as the use of a non-aqueous solvent like ethanol, as reported by Freni *et al.*,[33] or acidification of the precursor solution by HNO_3 addition, were not effective to improve metal penetration inside the pellet. Moreover, MgO pellets also showed some stability issues, testified by a BET surface area of 13 m^2 g^{-1} as provided by the supplier that increased up to 34 m^2 g^{-1} when calcined at 450 °C, but decreased to 27 m^2 g^{-1} when calcined at 600 °C.

A metal surface enrichment was also detected when either Ni (or Ru) were dispersed on *x*Mg/Al pellets, although possibly to a lower extent, as shown in Fig. 4b and b′ for the exemplificative case of Ni.

Takehira *et al.* also reported an egg-shell metal distribution when Ni was impregnated from nitrate solution onto MgO–$MgAl_2O_4$ mixed oxides, and attributed this effect to the rapid formation of a Mg(Ni)–Al hydrotalcite-like dense layer.[30,31]

Qiu *et al.*[29] found that the penetration rate of $Ni(NO_3)_2$ solution was three times less for MgO/Al_2O_3 spheres pre-calcined at 450 °C rather than at 650 °C, thus favouring an egg shell nickel distribution. On the other hand, they also reported that a further increase of calcination temperature of the support resulted in the formation of $MgAl_2O_4$ spinel with an increase of pore diameter favouring Ni^{2+} diffusion.[29]

In order to prevent the formation of phases (in particular MgO) inhibiting the diffusion of the active metal deep into the pores, Ni and Mg were simultaneously co-impregnated on γ-Al_2O_3 pellets from an aqueous solution of both nitrate precursors. This procedure gave very satisfactory results in terms of uniform distribution of nickel (as well as Mg) across the entire body of the alumina pellets, as shown by the corresponding SEM/EDX elemental maps of the pellet cross-section reported in Fig. 4c and c′.

Table 2 presents the textural features and surface basic properties of those catalytic pellets obtained after metal dispersion onto Mg/Al pellets pre-calcined at 600 °C. A comparison with corresponding data reported in Table 1 for Mg/Al supports first highlights an increase of the BET surface area obtained upon dispersion of either Ni or Ru, particularly evident with 20 Mg/Al pellets (*i.e.* those with larger MgO content). A similar effect was previously noticed when supporting the same metals on pure MgO powder and it was convincingly ascribed to a partial dissolution of MgO in water solution followed by a reconstruction of MgO surface.[13]

However, this contrasts to what observed by Carvalho *et al.*[23] for Ru dispersion from a chloride solution onto Al_2O_3, MgO and MgO–Al_2O_3 mixed oxides obtained from hydrotalcite-like precursor at the relatively low temperature of 450 °C, which was possibly too low to avoid some sintering during the calcination treatment following metal impregnation.

Fig. 5 presents XRD patterns of Ni/20Mg/Al and Ru/20Mg/Al calcined at 600 °C, in comparison with that relevant to their parent 20Mg/Al support calcined at the same temperature; standard oxide phases (MgO, Ru_2O and NiO) are also presented for reference. Notably, those signals at 42.9° and 62.3°, well detectable in the XRD patterns of 12 Mg/Al and 20 Mg/Al supports calcined at 600 °C and related to periclase MgO, almost disappeared in the metal-containing catalytic pellets.

Open Access Article. Published on 18 July 2018. Downloaded on 7/14/2025 8:34:56 AM.
This article is licensed under a Creative Commons Attribution-NonCommercial 3.0 Unported Licence.

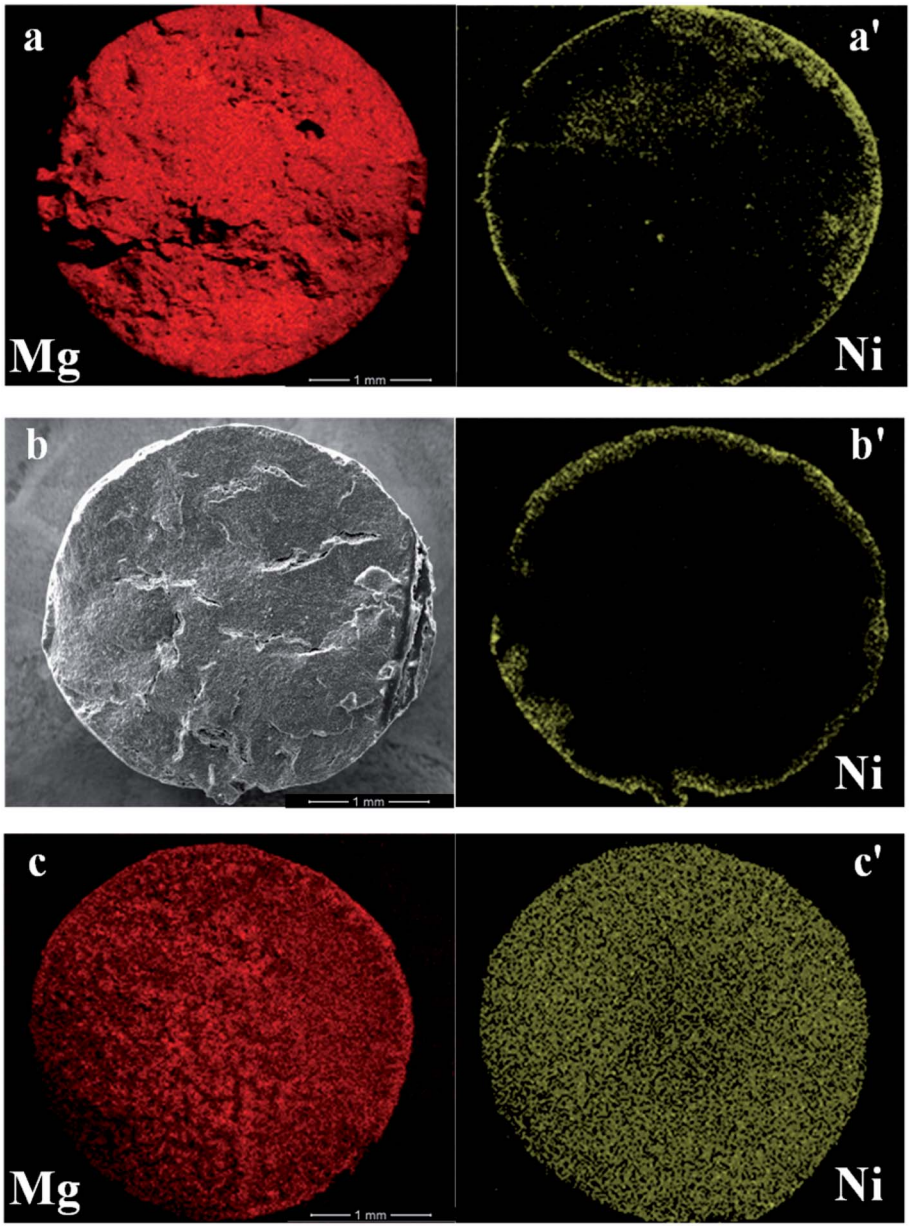

Fig. 4 SEM/EDX analysis with corresponding false-color elemental distribution across the section of catalytic pellets prepared by impregnation: (a and a′) Ni on MgO pellet; (b and b′) Ni on 12Mg/Al pellet; (c and c′) Ni/12Mg/Al pellet prepared by co-impregnation of alumina pellet with aqueous solution Mg and Ni nitrates.

Table 2 BET surface area and basic sites evaluated through CO_2 TPD of Me/Mg/Al pellets

Sample	BET surface area [$m^2\ g^{-1}$]	Pore volume [$cm^3\ g^{-1}$]	Basic sites CO_2 TPD [mmol g^{-1}]
Ni/12Mg/Al	155	0.68	0.35
Ni/12Mg/Al regen. 1	153	0.76	—
Ni/20Mg/Al	144	0.60	0.46
Ni/20Mg/Al co-impr.	128	0.67	0.31
Ru/20Mg/Al	125	0.51	0.38
Ru/20Mg/Al regen. 1	138	0.61	0.34
Ru/20Mg/Al regen. 3	152	0.59	—

This journal is © The Royal Society of Chemistry 2018

Open Access Article. Published on 18 July 2018. Downloaded on 7/14/2025 8:34:56 AM.
This article is licensed under a Creative Commons Attribution-NonCommercial 3.0 Unported Licence.

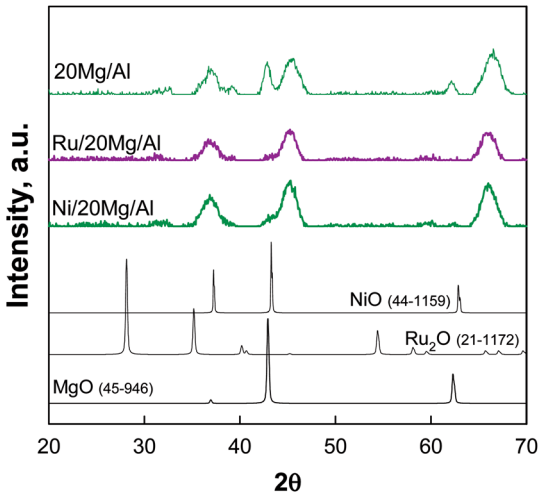

Fig. 5 XRD patterns of Ni/20Mg/Al and Ru/20Mg/Al catalytic pellets and their parent support calcined at 600 °C. Reference patterns for MgO (JCPDS 45-946), Ru_2O (JCPDS 21-1172) and NiO (JCPDS 44-1159) are displayed at the bottom.

This suggests the dissolution of the MgO phase during the water impregnation step and its eventual reconstruction with a lower crystallinity. A poorly resolved peak at *ca.* 43.2° appeared in the pattern of Ni/20Mg/Al catalyst and could be assigned to the presence of poorly crystalline NiO species. On the contrary, no diffraction peaks related to Ru oxide phases were detected for Ru/20 Mg/Al catalytic pellets calcined in air at 600 °C, probably due to a high metal dispersion and to the low metal loading. Similar findings were previously reported for 1% wt Ru supported on Al_2O_3, MgO and MgO–Al_2O_3 mixed oxides derived from a hydrotalcite-like precursor.[23,27] However, Ni and Ru inclusion in MgO as well as in the alumina structure is also possible.[23] Notably, ICP-MS analysis confirmed that the average Ni content in catalytic pellets was close to the nominal one (1% wt), whereas the content of Ru was as low as 0.02% wt, likely due to the extensive precipitation of Ru insoluble species during the impregnation step of *x*Me/Al pellets.

Fig. 6 shows H_2-TPR profiles recorded up to 900 °C for metal impregnated catalytic pellets. In the same temperature range, the corresponding supports were poorly reducible, as exemplified in the same figure by the almost flat TPR profile of 20Mg/Al pellets.

Ni-containing catalysts showed a generally higher hydrogen consumption, as also expected by the larger actual metal loading, but their TPR profiles were strongly influenced by the type of support and preparation strategy. In the case of Ni/12Mg/Al material, the main reduction event appeared with an onset temperature of *ca.* 550 °C and a peak at 780 °C, followed by a second peak at 900 °C, the latter being concluded under the isothermal stage. Ni/20Mg/Al catalyst showed one single broader peak with identical onset temperature but centred at 870 °C, which reasonably resulted from the partial overlap of two contributions similar to those observed for Ni/12Mg/Al. Both catalysts showed some additional small signals in the temperature range 350–600 °C which can be attributed to the reduction of Ni^{2+} in the NiO phase.[34] On the contrary, according

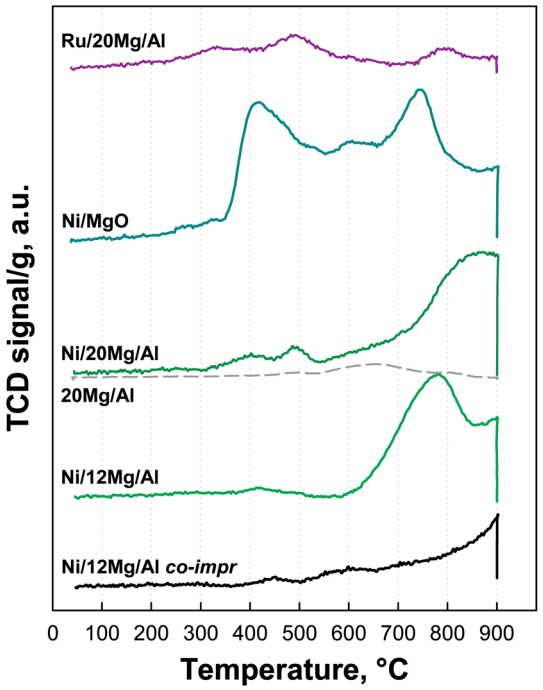

Fig. 6 TPR profiles of Me/*x*Mg/Al and Ni/MgO catalytic pellets calcined at 600 °C.

to literature data, the reduction of Ni^{2+} species in mixed phases with MgO and Al_2O_3 occurred in a significantly higher temperature range (600–1000 °C)[35] and thus was not completed at 900 °C (as in our experiments). In particular, for the case of a NiMgAl sample calcined at 1000 °C, Villa *et al.* reported two TPR peaks centred at 720 and 1000 °C, associated with the reduction of Ni^{2+} in the mixed phases $Ni_{1-x}Mg_xO$ and $Ni_{1-y}Mg_yAl_2O_4$, respectively.[34] Gac *et al.* also presumed the formation of a solid solution resulting into a decrease of metal reducibility measured by H_2 TPR with increasing MgO content for co-precipitated Ni–MgO–Al_2O_3 catalysts.[21] Likewise, Koo *et al.* observed Ni reduction at 600–700 °C supposing the formation of a solid solution with the MgO/Al_2O_3 support for a Ni load as high as 50%.[20] Notably, when Ni and Mg were uniformly distributed throughout alumina pellets *via* the co-impregnation procedure, only one high temperature reduction peak was observed, which was not completed during the isothermal stage at 900 °C (Fig. 6), thus suggesting the extensive formation of $Ni_{1-y}Mg_yAl_2O_4$ solid solution.[33]

Eventually, Ni/MgO pellets also showed two main reduction peaks centred at *ca.* 415 and 745 °C, that can be assigned to the reduction of Ni^{2+} in NiO and in $Ni_{1-x}Mg_xO$ solid solution, respectively. Likewise, Parmaliana *et al.* observed two analogous peaks in their TPR curves of NiO–MgO samples and reported that calcination at high temperature for a long time of Ni/MgO samples at low Ni loading promoted the inclusion of Ni^{2+} ions into the MgO lattice.[18]

The shoulder in between those peaks was probably associated with the decomposition of some Mg carbonate species formed during the heat treatment in air following Ni deposition on the MgO pellets.

Open Access Article. Published on 18 July 2018. Downloaded on 7/14/2025 8:34:56 AM.
This article is licensed under a Creative Commons Attribution-NonCommercial 3.0 Unported Licence.

In contrast to Ni containing catalysts, Ru-based pellets displayed a limited H_2 consumption, due to their rather low actual metal loading. In particular, two small, broad and partially overlapping peaks in the temperature ranges 210–400 and 400–600 °C, could be assigned respectively to the reduction of supported Ru_2O species with different degree of interaction with the Mg/Al support,[36] and to some carbonate decomposition or even hydrogen spillover from the metal to the support itself.

As already mentioned, Takehira *et al.* reported that when their Mg–Al mixed oxide support prepared at 450 °C was dipped into a Ni^{2+} nitrate aqueous solution, a Mg–Al hydrotalcite type phase was formed containing Ni^{2+} in the Mg^{2+} site.[31] In agreement with the present results, the same authors also observed an eggshell-type distribution of Ni, resulting from the fast formation rate of this Mg(Ni)–Al hydrotalcite phase on the outer surface layer that hinders the penetration rate of Ni^{2+} nitrate aqueous solution deep into the pores. In fact, if the calcination temperature of the mixed Mg–Al support was high enough to turn all the superficial MgO into $MgAl_2O_4$ spinel (*i.e.* 900 °C), the mixed Mg(Ni)–Al was not formed and a uniform distribution of Ni in the catalytic pellets was obtained. Accordingly, the formation of a NiO–MgO solid solution with the substitution of Ni^{2+} ions in Mg^{2+} sites was reported by Yoshida *et al.* for MgO powder catalysts prepared by impregnation from nickel nitrate aqueous solution.[19]

CO_2-TPD profiles of Me/*x*Mg/Al catalytic pellets (Fig. 7) resembled those relevant to their parent supports, indicating that metal addition had a limited effect on the distribution and strength of surface basic sites of the materials. However, a small but detectable increase in the number of basic sites with respect to its support was recorded only for Ni/20Mg/Al catalyst (Table 2) containing the highest amount of MgO. In agreement, impregnation of Ni on pure MgO powder was previously found to induce an increase of CO_2-adsorption due to partial dissolution and reconstruction of the support.[13] On the other hand, the catalyst prepared by co-impregnation of Ni and Mg onto alumina pellets displayed a significant reduction in the number of basic sites (−33%, Table 2) with respect to its counterpart with identical nominal composition obtained by sequential impregnations, which agrees with the extensive formation of $Ni_{1-y}Mg_yAl_2O_4$ solid solution already inferred by TPR analysis.

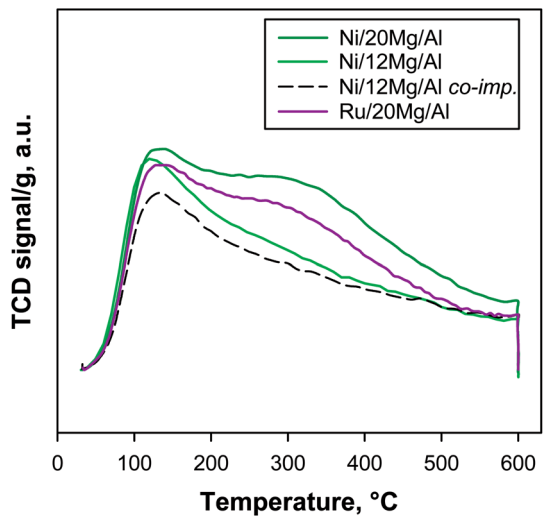

Fig. 7 CO_2 TPD profiles of Me/*x*Mg/Al catalysts prepared by sequential impregnation of Ni or Ru onto *x*Mg/Al pellets and a Ni/12 Mg/Al sample prepared by co-impregnation of Ni and Mg onto alumina pellets.

3.3 Catalytic activity

Fig. 8 reports experimental data of butanol yield and ethanol conversion obtained during catalytic tests carried out at 350 and 400 °C with selected catalytic pellets and supports prepared in this work.

All of the pellets can activate ethanol and produced, in addition to butanol, variable amounts of ethylene/diethylether, acetaldehyde and traces of crotonaldehyde. Notably, 12Mg/Al pellets calcined at 900 °C provided a very high ethanol conversion (*ca.* 80% at 400 °C), but produced rather low amounts of butanol (yield < 1%), showing a behavior corresponding to that previously reported for pure alumina under similar operating conditions which provided ethanol conversion close to 100%, mostly converting it to ethylene/diethylether.[13] This is in agreement with results of characterization showing that 12Mg/

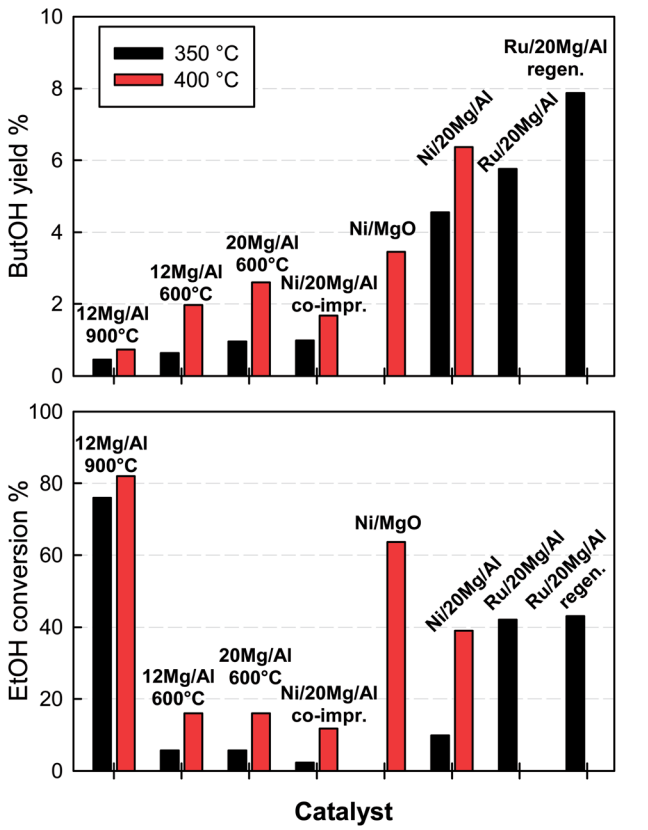

Fig. 8 Comparison of butanol yield and ethanol conversion data obtained during catalytic tests of Guerbet reaction run at 350 and 400 °C with selected materials. Ru/20Mg/Al and Ni/MgO catalysts were tested only at 350 and 400 °C, respectively. Feed: EtOH 3% in N_2.

This journal is © The Royal Society of Chemistry 2018

Open Access Article. Published on 18 July 2018. Downloaded on 7/14/2025 8:34:56 AM.
This article is licensed under a Creative Commons Attribution-NonCommercial 3.0 Unported Licence.

Al calcined at 900 °C has features similar to Al_2O_3 because of the formation of a surface Mg-aluminate spinel. Therefore, the lack of strong basic sites found for this catalyst favors those reactions leading to heavier organic compounds which, in contrast, are inhibited by a higher surface basicity.[14] On the contrary, 12Mg/Al pellets calcined at 600 °C, showed a better activity towards butanol production, giving a 2% butanol yield at 400 °C in correspondence of a much lower ethanol conversions (16%). The larger MgO content in 20Mg/Al pellets slightly enhanced the butanol yield up to 2.6% at 400 °C in correspondence to a similar ethanol conversion. Such results show that the coverage of alumina with a superficial layer of magnesium oxide, already at 12% wt of MgO, is enough to suppress the high ability of alumina to activate ethanol towards the formation of by-products[13] rather than of butanol. This is related to the partial neutralization of acid sites and to the additional formation of strong basic sites provided by MgO, which, according to Birky *et al.*,[14] promote the production of butanol through the occurrence of a coupling reaction giving an aldol condensation.

Metal impregnated catalytic pellets generally outperformed their parent supports. The only exception was represented by Ni/12Mg/Al catalyst prepared by co-impregnation of Ni and Mg onto alumina pellets, whose butanol yield (*ca.* 1.7% at 400 °C) and ethanol conversion closely resembled those obtained with the corresponding support without Ni. Indeed this is not surprising recalling that H_2-TPR analysis of this sample had shown Ni was mostly contained in solid solution with alumina ($NiAl_2O_4$) and the surface basic features assessed by CO_2-TPD resembled those of *x*Mg/Al pellets calcined at 600 °C. Ni/MgO pellets provided a butanol yield of *ca.* 3.5% at 400 °C (EtOH conversion *ca.* 63%), quite similar to the value obtained over the corresponding Ni/MgO powder catalyst:[13] in fact, some small differences noticed in catalytic performance between the two samples do not correspond to the significant variation in the total surface area for the same nominal composition (75 $m^2\ g^{-1}$ for powder and 29 $m^2\ g^{-1}$ for pellets). The addition of nickel to *x*Mg/Al pellets calcined at 600 °C strongly improved butanol yield and ethanol conversion at both temperature levels: a maximum yield of *ca.* 6.5% was achieved with Ni/20Mg/Al pellets at 400 °C in correspondence of a 40% conversion of ethanol. Notably, also in this case the results (specifically in terms of EtOH conversion) do not correlate to the larger surface area of Ni/20Mg/Al with respect to Ni/MgO, but they rather reflect the strong difference of reducibility of Ni^{2+} species found by TPR analysis (Fig. 6) highlighting the importance of the interaction between Ni and MgO and the formation of a solid solution.[18,21] It can be argued that the mixed $Ni_{1-x}Mg_xO$ phases, formed on the surface of the Ni/*x*Mg/Al pellets, displays the highest selectivity towards butanol production. On the contrary, NiO species, which are also formed in a significant amount on the surface of Ni/MgO catalysts together with $Ni_{1-x}Mg_xO$, tend to activate more effectively those undesired reactions of ethanol towards products such as acetaldehyde and ethylene possibly due to their easier reducibility (already at 350 °C during H_2 TPR).

The pronounced egg-shell metal distribution of the present catalytic pellets derived from the strong basic nature of their supported MgO species, which are beneficial to activate the Guerbet reaction. Nevertheless, the effect of a different, more uniform, metal distribution (and the way to obtain it) will deserve further investigation.

Dispersion of ruthenium rather than nickel over 20Mg/Al pellets provided even better catalytic results, despite the quite low metal loading achieved in this catalyst. In particular, the maximum butanol yield obtained with Ru/20Mg/Al and Ni/20Mg/Al pellets were similar (as well as ethanol conversion), but operating the Ru-based catalyst at the lower temperature of 350 °C. This confirms a key role of the metal in the Guerbet reaction. Indeed, the initial dehydrogenation of the adsorbed ethanol molecule to give the ethoxy intermediate responsible for the subsequent aldol condensation[14,15] can be favoured by the presence of a metal. The good performance of Ru-based catalysts seems again associated to the formation of a mixed phase, possibly a spinel-like phase, as also found by Li *et al.*[27] for Ru–Mg–Al–O catalyst calcined at 600 °C, and in agreement with the H_2-TPR results in this work.

Notably, butanol yield data previously reported by other groups operating under diluted ethanol feed conditions with pure MgO or mixed Mg–Al formulations were always limited to below 5%.[16,37] However, Ni or Ru doping of our *x*Mg/Al pellets was effective to enhance butanol formation with maximum measured yields around 7–8% (Fig. 8).

The average duration of a catalytic test was about 4 hours. After 30–40 min activation the catalyst achieved stable performance up to the end of the experiment. Nevertheless, after the catalytic tests pellets became visibly darker, most likely due to the deposition some heavier organic by-products and/or coke. Therefore, though not strictly required, catalytic pellets were regenerated by repeating a 2 h calcination treatment under an air flow at 600 °C. Thereafter, specific surface area measurements and catalytic reaction tests were repeated to assess the stability of the regenerated catalysts.

The BET surface area of Ni-based catalysts remained substantially unchanged after the regeneration treatment at 600 °C, and the catalytic performance was not affected as well. Somehow surprisingly, Ru/20 Mg/Al catalyst showed a progressive increase of its specific surface area along with the number of regeneration treatments from 125 $m^2\ g^{-1}$ for the fresh sample and up to 152 $m^2\ g^{-1}$ after 3 calcination cycles at 600 °C (Table 2). At the same time, an improvement of the catalytic performance was also observed, testified by the increase in butanol yield from *ca.* 6 to almost 8%, achieved without any significant variation in the conversion of ethanol (Fig. 8).

A possible explanation for the increase of surface area is that the combustion of organics on the catalyst surface could involve a local over-heating at temperatures above 600 °C. Obviously, such an effect cannot occur during the preparation of impregnated pellets, since calcination promotes only the endothermic decomposition of nitrate precursors.[38] To check this hypothesis, Ru-based pellets initially calcined at 600 °C were further treated at 650, 700 and 800 °C. It was found that calcination at 650 and 700 °C increased the surface area of samples (154 and 143 m^2

Open Access Article. Published on 18 July 2018. Downloaded on 7/14/2025 8:34:56 AM. This article is licensed under a Creative Commons Attribution-NonCommercial 3.0 Unported Licence.

g^{-1} respectively), whereas heating at 800 °C significantly reduced it (88 m^2 g^{-1}). Butanol yield obtained for the catalyst calcined at 650 °C (7.6%) was close to that of the regenerated sample, but it decreased to *ca.* 3% and 1.8% after calcination at 700 and 800 °C, respectively. Eventually, it can be argued that the calcination temperature should be high enough to promote the extensive formation of the metal-MgO solid solution, but not too high to favour the formation of Mg-aluminate phase with the consequent loss of MgO features. Nevertheless, the regeneration process seems more complex than a simple calcination at a higher temperature and further investigation is necessary.

4. Conclusions

Nickel and ruthenium supported on MgO-coated γ-alumina pellets were prepared, characterized and tested for the conversion of ethanol into butanol. The preparation conditions were deeply investigated in order to define those providing catalytic pellets preserving the high surface of γ-Al_2O_3 but showing the basic surface properties of MgO, which is intrinsically much more active and selective towards butanol production than alumina.

Calcination at 600 °C of alumina pellets impregnated with Mg nitrate allowed decomposition of the precursor to form dispersed MgO species while preventing the significant formation of an aluminate-like structure associated with poor catalytic performance.

The contact of active metals such as Ni or Ru with MgO covered Al_2O_3 pellets followed by calcination at 600 °C in air promoted the formation of a solid solution which is responsible for a very good butanol production. Simultaneous addition of metal and Mg on alumina pellets led to the undesired preferential interaction of the metal with the Al_2O_3 lattice.

The structured catalysts showed a uniform distribution of MgO throughout the pellets but a marked egg-shell distribution of the active metal (Ni or Ru), with a rather limited penetration length caused by partial dissolution of MgO during the impregnation step causing the fast precipitation of insoluble mixed metal-Mg species.

During reaction tests with diluted ethanol feed at 350–400 °C, Me/*x*Mg/Al catalytic pellets gave maximum butanol yields ranging from 6 up to 8% that are significantly higher than values previously reported in the literature for undoped MgO or hydrotalcite-derived mixed Mg–Al materials, as well as for Ni/MgO catalysts (either in powder form or pellets), in spite of a lower loading of MgO in the reactor.

Moreover, Me/*x*Mg/Al pellets showed rather stable performance during the reaction as well as after regeneration treatments at 600 °C in air to burn out carbon deposits. In fact, those repeated oxidative treatments turned out to slightly increase the performance of Ru-based systems with a simultaneous enhancement of the surface area.

These results highlight the positive effect of increased MgO dispersion onto alumina and also the very good stability related to the interaction with the alumina substrate and with the dispersed metal.

Conflicts of interest

There are no conflicts to declare.

Acknowledgements

The work has been done in the framework of the Research project Waste2Fuels 'Sustainable Production of Next Generation Biofuels from Waste Streams' (No. 654623) funded under the European Union's Research and Innovation Program Horizon 2020. Authors are grateful to Mr Luciano Cortese for SEM/EDX analysis, Mr Andrea Bizzarro for N_2-physisorption analysis and Mr Ferdinando Stanzione for ICP/MS analysis.

References

1 A. D. Patel, S. Telalović, J. H. Bitterb, E. Worrell and M. K. Patel, *Catal. Today*, 2015, **239**, 56–79.
2 J. Sun and Y. Wang, *ACS Catal.*, 2014, **4**, 1078–1090.
3 J. H. Earley, R. A. Bourne, M. J. Watson and M. Poliakoff, *Green Chem.*, 2015, **17**, 3018–3025.
4 A. S. Ndou, N. Plint and N. J. Coville, *Appl. Catal., A*, 2003, **251**, 337–345.
5 T. Riittonen, E. Toukoniitty, D. Kumar Madnani, A. R. Leino, K. Kordas, M. Szabo, A. Sapi, K. Arve, J. Wärnå and J. P. Mikkola, *Catalysts*, 2012, **2**, 68–84.
6 T. Tsuchida, S. Sakuma, T. Takeguchia and W. Ueda, *Ind. Eng. Chem. Res.*, 2006, **45**, 8634–8642.
7 T. Tsuchida, J. Kuboa, T. Yoshioka, S. Sakuma, T. Takeguchi and W. Ueda, *J. Catal.*, 2008, **259**, 183–189.
8 S. Ogo, A. Onda and K. Yanagisawa, *Appl. Catal., A*, 2011, **402**, 188–195.
9 J. L. M. Gines and E. Iglesia, *J. Catal.*, 1998, **176**, 155–172.
10 W. Ueda, T. Kuwabara, T. Ohshida and Y. A. Morikawa, *J. Chem. Soc., Chem. Commun.*, 1990, 1558–1559.
11 I.-C. Marcu, D. Tichit, F. Fajula and N. Tanchoux, *Catal. Today*, 2009, **147**, 21–238.
12 D. L. Carvalho, R. R. de Avillez, M.-T. Rodrigues, L. E. Borges and L. G. Appel, *Appl. Catal., A*, 2012, **415**, 96–100.
13 S. Cimino, L. Lisi and S. Romanucci, *Catal. Today*, 2018, **304**, 58–63.
14 T. W. Birky, J. T. Kozlowski and R. J. Davis, *J. Catal.*, 2013, **298**, 130–137.
15 J. T. Kozlowski and R. J. Davis, *ACS Catal.*, 2013, **3**, 1588–1600.
16 A. Chieregato, J. Velasquez Ochoa, C. Bandinelli, G. Fornasari, F. Cavani and M. Mella, *ChemSusChem*, 2015, **8**, 377–388.
17 M. León, E. Díaz and S. Ordóñez, *Catal. Today*, 2011, **164**, 436–442.
18 A. Parmaliana, F. Arena, F. Frusteri and N. Giordano, *J. Chem. Soc., Faraday Trans.*, 1990, **86**, 2663–2669.
19 T. Yoshida, T. Tanaka, H. Yoshida, T. Funabiki and S. Yoshida, *J. Phys. Chem.*, 1996, **100**, 2302–2309.
20 K. Y. Koo, M. G. Park, U. H. Jung, S. H. Kim and W. L. Yoon, *Int. J. Hydrogen Energy*, 2014, **39**, 10941–10950.

 This journal is © The Royal Society of Chemistry 2018

Open Access Article. Published on 18 July 2018. Downloaded on 7/14/2025 8:34:56 AM.
This article is licensed under a Creative Commons Attribution-NonCommercial 3.0 Unported Licence.

21 W. Gac, A. Denis, T. Borowiecki and L. Kępiński, *Appl. Catal., A*, 2009, **357**, 236–243.
22 B. Yue, X. Wang, X. Ai, J. Yang, L. Li, X. Lu and W. Ding, *Fuel Process. Technol.*, 2010, **91**, 1098–1104.
23 L. S. Carvalho, A. R. Martins, P. Reyes, M. Oportus, A. Albonoz, V. Vicentini and M. do Carmo Rangel, *Catal. Today*, 2009, **142**, 52–60.
24 A. C. Basagiannis and X. E. Verykios, *Catal. Today*, 2007, **127**, 256–264.
25 A. C. Basagiannis and X. E. Verykios, *Appl. Catal., B*, 2008, **82**, 77–88.
26 B. Nematollahi, M. Rezaei and M. Khajenoori, *Int. J. Hydrogen Energy*, 2011, **36**, 2969–2978.
27 L. D. Li, J. J. Yu, Z. P. Hao and Z. P. Xu, *J. Phys. Chem. C*, 2007, **111**, 10552–10559.
28 X. Ju, L. Liu, P. Yu, J. Guo, X. Zhang, T. He, G. Wu and P. Chen, *Appl. Catal., B*, 2017, **211**, 167–175.
29 Y. Qiu, J. Chen and J. Zhang, *React. Kinet. Catal. Lett.*, 2008, **94**, 149–155.
30 K. Takehira, T. Shishido, D. Shoro, K. Murakami, M. Honda, T. Kawabata and K. Takaki, *Catal. Commun.*, 2004, **5**, 209–213.
31 K. Takehira, T. Kawabata, T. Shishido, K. Murakami, T. Ohi, D. Shoro, M. Honda and K. Takaki, *J. Catal.*, 2005, **231**, 92–104.
32 P. Fu, W. Lu, W. Lei, K. Wu, Y. Xu and J. Wu, *Mater. Res.*, 2013, **16**, 844–849.
33 S. Freni, S. Cavallaro, N. Mondello, L. Spadaro and F. Frusteri, *Catal. Commun.*, 2003, **4**, 259–268.
34 R. Villa, C. Cristiani, G. Groppi, L. Lietti, P. Forzatti, U. Cornaro and S. Rossini, *J. Mol. Catal. A: Chem.*, 2003, **204–205**, 637–646.
35 S. De, J. Zhang, R. Luque and N. Yan, *Energy Environ. Sci.*, 2016, **9**, 3314–3347.
36 X. Ju, L. Liu, P. Yu, J. Guo, X. Zhang, T. He, G. Wu and P. Chen, *Appl. Catal., B*, 2017, **211**, 167–175.
37 S. Hanspal, Z. D. Young, H. Shou and R. J. Davis, *ACS Catal.*, 2015, **5**, 1737–1746.
38 R. A. J. Sietsma, H. Friedrich, A. Broersma, M. Versluijs-Helder, A. J. van Dillen, P. E. de Jongh and K. P. de Jong, *J. Catal.*, 2008, **260**, 227–235.